Environ. Sci. Technol. **1999**, *33,* 276−281

Surface Chemical Characteristics of Coal Fly Ash Particles after Interaction with Seawater under Natural Deep Sea Conditions

YANIV BRAMI,[†] BARAK HERUT,*[,‡] ALDO SHEMESH,[†] AND HAGAI COHEN[§]

Department of Environmental Sciences and Energy Research, Weizmann Institute of Science, Rehovot 76100, Israel, Israel Oceanographic & Limnological Research, National Institute of Oceanography, Tel-Shikmona, P.O. Box 8030, Haifa 31080, Israel, and Chemical Services Unit, Weizmann Institute of Science, Rehovot 76100, Israel

The surface (0.2−0.5 nm) chemical characteristics of coal fly ash (CFA) before and after interaction with Mediterranean deep seawater was studied by X-ray photoelectron spectroscopy (XPS). Significantly lower values of Si, Ca, and S and higher values of Mg and Cl were found in the retrieved CFA as compared to fresh CFA. It is suggested that hydrolysis of the oxide matrixes results in an alkaline environment which rapidly leads to several chemical reactions. The two most important are (a) dissolution of the amorphous silicate and the calcium phases and (b) precipitation of $Mg(OH)_2$−brucite. A depth profile of the retrieved CFA was measured by both line-shape analysis of the XPS spectra and by consecutive cycle of sputtering. The thickness of the brucite layer is estimated to be 1.3 nm.

Introduction

Power plants, which rely on coal as an energy source, have led to a management problem related to the storage and disposal of coal fly ash (CFA). The option of deep sea disposal was recognized as an attractive opportunity for coastal power plants (*1, 2*). However, an environmental concern may rise due to the potential availability of toxic elements (Cd, Pb, Zn, Cu, As, Se, and Cr) released from CFA to the marine environment. The leaching of elements from CFA into seawater is controlled by solubility processes (*3, 4*); therefore, identification of mechanisms governing the leaching processes is an important step for comprehending the role of CFA interactions with seawater. To present, leaching of CFA in seawater and in freshwater was studied under different conditions, such as pH, solid-to-liquid ratio, and exposure time (*5*−*7*). Many laboratory experiments and field measurements were performed to investigate bulk chemical variations due to the interaction between CFA and seawater (*1, 2, 4, 7*−*9*). These laboratory experiments had short duration and could not account for the effects of long-term aging and weathering processes that might occur under natural deep sea conditions. The comprehension of long-term aging and weathering processes that might occur to CFA is facilitated by utilizing surface sensitive techniques such as XPS (*10, 11*).

Extensive studies using XPS for surface characterization of fresh CFA were conducted in the past (*12*−*16*). These studies suggested that volatilization−condensation mechanisms may result in the enrichment of the elements Ca, P, S, and Mg on the CFA particle surfaces. To the best of our knowledge, no studies have been carried out on changes in the surface chemical composition of CFA particles retrieved after a long duration under natural deep sea conditions. In the present study, CFA dumped to the southeastern Mediterranean since 1982 was retrieved and its surface characteristics, chemical composition, and morphology were compared with the original fresh CFA produced at the power plant. XPS was used to characterize the surface chemical composition of the CFA particles. Scanning electron microscopy coupled with energy dispersive spectroscopy (SEM/EDS) were used to identify particle morphology and elemental composition of discrete particles.

Experimental Section

Since 1982, more than one million tons of CFA were disposed into a deep (1400 m) dump site located 70 km off the Israeli Mediterranean coast (*7*). CFA samples were retrieved (RCFA) from the dump site during January 1995 on board of R/V *Shikmona* (Stations A and P9). The temperature and salinity monitored at the sampling station were 13.70 ± 0.10 °C and 38.68 ± 0.04 ‰, respectively. Sediment samples containing CFA were sampled using a BX 700AL box corer and CFA pebbles were retrieved using a beam trawl. The exact exposure time of these samples to seawater is not known and is probably in the range of 1−3 years. The upper layer of the sediment (approximately 1 cm) was mostly fine grained CFA particles and aggregates which were picked up and stored with the pebbles in 4 °C prior analysis. The CFA physical characteristics are given in ref *7*. Twenty RCFA aggregates (<2 cm diameter) were thoroughly washed with double distilled water. Their outer 2−3 mm was removed and sieved through 45 μm. Representative fresh CFA (FCFA) samples from the Hadera Electricity Power Station were used for comparison. These composite samples represent an average of a period of a six-month period of production and were treated similarly to the RCFA samples. A further size fractionation to particles smaller than 25 and 5 μm was conducted for the representative FCFA and RCFA samples by a conventional method using cylinders of 5 cm diameter and 80 cm long. The suspension was centrifuged at 2000 rpm, and <5 μm particles were separated from the suspension. As given hereafter, to assess possible affect of this pretreatment on differential dissolution of certain phases we used Al as a conservative element. The particle size of each group was also confirmed by scanning electron microscopy (SEM) screening.

X-ray powder diffraction (XRD) was used for the mineralogical analyses. Particle morphology and bulk chemical composition were studied by Philips 505 SEM/EDX. Kratos Analytical AXIS-HS XPS was used to study the surface chemical composition of the particles. A typical 0.5−0.2 nm surface layer was analyzed by a 2-mm-diameter beam which encompasses hundreds of particles and therefore represents an average composition of the surface layer. In the present study, a new sample holder was designed to solve the problems associated with the particles suspension. The sample holder was constructed of gold-coated stainless steel

* Corresponding author telephone: +972-4-8515202; fax: +972-4-8511911; e-mail address: barak@ocean.org.il.

[†] Department of Environmental Sciences and Energy Research, Weizmann Institute of Science.

[‡] National Institute of Oceanography.

[§] Chemical Services Unit, Weizmann Institute of Science.

10.1021/es9805573 CCC: $18.00
Published on Web 12/10/1998

TABLE 1. XPS Surface Composition of Representative Fresh Coal Fly Ash (Atomic %)

sample no.	month	year	fraction	Al(2s)	Si(2p)	Ca(2p)	Fe(2p)	Ti(2p)	S(2p)	Mg(2s)	P(2p)	K(2p)	Na(1s)	Cl(2p)	O(1s)	C(1s)
1	7−12	1989	<45 μm	7.39	10.68	3.59	0.84	0.37	1.47	1.45	1.43	0.37	0.23	nd[a]	56.04	16.14
2	7−12	1989	<45 μm	7.56	10.52	3.66	0.73	0.32	1.82	2.75	1.07	0.41	0.19	nd	57.49	13.49
3	7−12	1991	<45 μm	7.39	9.70	3.61	0.54	0.25	0.80	2.04	0.96	0.22	0.11	0.21	52.12	22.05
4	7−12	1991	<45 μm	5.76	7.11	4.88	0.55	0.29	0.82	2.51	0.41	0.14	0.12	0.26	46.77	30.37
5	1−6	1991	<45 μm	6.12	9.86	5.97	0.65	0.41	0.89	1.70	0.92	0.19	0.09	0.36	51.66	21.12
average				**6.84**	**9.57**	**4.34**	**0.66**	**0.33**	**1.16**	**2.09**	**0.96**	**0.27**	**0.15**	**0.28**	**52.82**	**20.63**
SD				0.84	1.44	1.06	0.13	0.06	0.46	0.54	0.37	0.12	0.06	0.08	4.20	6.49

[a] nd = not determined.

TABLE 2. XPS Surface Composition of Retrieved Coal Fly Ash (Atomic %)

sample no.	station	agregate size	fraction	Al(2s)	Si(2p)	Ca(2p)	Fe(2p)	Ti(2p)	S(2p)	Mg(2s)	P(2p)	K(2p)	Na(1s)	Cl(2p)	O(1s)	C(1s)
12	station P9	<2 cm	<45 μm	6.03	6.20	1.60	1.34	0.31	0.60	10.06	0.86	0.47	1.17	4.03	53.23	14.11
13	station P9	<2 cm	<45 μm	7.67	5.93	1.97	0.50	0.20	0.71	9.58	1.09	0.21	0.87	1.78	58.92	10.64
14	station P9	<2 cm	<45 μm	5.36	6.34	2.05	0.71	0.24	0.55	9.23	0.56	0.31	1.03	3.10	56.75	13.79
15	station P9	<2 cm	<45 μm	6.00	6.71	1.72	0.78	0.28	0.55	9.36	0.72	0.21	0.60	1.74	57.28	14.08
25	station P9	2 × 3 mm	<45 μm	6.83	9.99	0.74	1.27	0.46	nd[a]	8.10	0.60	0.43	1.15	3.18	52.00	15.30
26	station P9	4 × 5 mm	<45 μm	7.59	7.49	2.90	1.07	0.26	0.48	6.28	1.50	0.44	1.06	1.62	58.92	10.39
27	station P9	<2 cm	<45 μm	5.93	6.06	0.74	0.69	0.21	0.61	9.86	0.34	0.15	0.43	1.08	57.80	16.10
19	station A	<2 cm	<45 μm	6.41	5.38	1.83	0.82	0.32	0.85	8.77	0.61	0.15	1.03	2.47	56.39	15.00
20	station A	<2 cm	<45 μm	6.59	6.17	2.07	1.91	0.33	0.54	8.63	0.86	0.22	1.23	2.89	56.01	12.70
21	station A	<2 cm	<45 μm	6.43	6.06	2.22	0.73	0.36	0.43	9.58	0.69	0.18	0.81	1.69	56.65	14.09
31	station A	1 cm	<45 μm	7.93	6.02	4.73	1.41	0.25	1.35	12.49	1.41	0.29	1.45	3.71	54.26	nd
33	station A	3 cm	<45 μm	5.96	7.19	0.78	0.51	0.25	0.71	11.84	0.50	0.11	0.64	1.52	56.38	13.60
34	station A	3 cm	<45 μm	6.12	6.93	0.75	0.72	0.34	0.68	11.72	0.45	0.13	0.51	1.26	56.49	13.88
37	trawl	25 × 17 × 13 cm	<45 μm	6.02	7.55	0.55	1.02	0.26	0.38	10.97	0.41	0.11	0.48	0.61	60.16	11.50
38	trawl	25 × 17 × 13 cm	<45 μm	6.79	7.29	0.62	1.11	0.19	0.65	11.39	0.38	0.18	0.14	0.60	60.32	10.37
average				**6.51**	**6.75**	**1.68**	**0.97**	**0.28**	**0.65**	**9.86**	**0.73**	**0.24**	**0.84**	**2.09**	**56.77**	**13.25**
SD				0.74	1.10	1.11	0.39	0.07	0.24	1.63	0.36	0.12	0.36	1.08	2.35	1.86
16	station P9	<2 cm	<20 μm	7.64	7.00	1.27	0.76	0.30	0.65	9.01	0.86	bdl[b]	0.44	0.40	58.04	13.62
22	station A	<2 cm	<20 μm	7.15	6.61	1.43	0.88	0.26	0.33	9.73	0.74	0.09	0.18	0.17	60.30	12.12
average				**7.40**	**6.81**	**1.35**	**0.82**	**0.28**	**0.49**	**9.37**	**0.80**	**0.09**	**0.31**	**0.29**	**59.17**	**12.87**
SD				0.34	0.27	0.11	0.08	0.03	0.23	0.50	0.09		0.18	0.16	1.60	1.06
17[c]	station P9	<2 cm	<5 μm	2.46	1.93	1.03	0.10	bdl	0.28	1.90	0.63	bdl	0.11	0.14	39.18	52.17
18[c]	station P9	<2 cm	<5 μm	2.51	2.10	nd	nd	nd	0.10	3.05	0.67	nd	nd	0.39	32.39	58.33
23	station A	<2 cm	<5 μm	8.01	5.72	nd	1.09	0.39	0.17	8.16	1.30	0.05	0.06	bdl	66.21	8.79
24	station A	<2 cm	<5 μm	8.71	5.87	1.49	0.93	0.40	0.26	8.57	1.25	0.01	0.17	bdl	63.66	8.55
average				**5.42**	**3.91**	**1.26**	**0.71**	**0.40**	**0.20**	**5.42**	**0.96**	**0.03**	**0.11**	**0.27**	**50.36**	**31.96**
SD				3.40	2.18	0.33	0.53	0.01	0.08	3.44	0.36	0.03	0.05	0.18	17.09	27.01

[a] nd = not determined. [b] bdl = below detection limit (were not included in the average calculations). [c] The high carbon content is probably of marine origin.

with two holes where the CFA suspension was inserted. Prior to the analysis, the stub was placed in an oven at 105 °C overnight. The sample holder was then inserted into the XPS vacuum chamber for 6 more hours until the vacuum reached 10^{-8} Torr.

An Ar^+ ion beam was used with the XPS analysis to etch particle surfaces. A sputtering procedure was performed to examine the composition profile from the surface to a depth of approximately 400 Å. It was assumed that approximately 40 Å of the surface is removed upon exposure to 1 min of sputtering.

Measurements of different subsamples indicate that XPS data are reproducible within ±3% for the major elements. These differences may be attributed to the variability within the original CFA sample and the XPS accuracy.

Results and Discussion

X-ray powder diffraction of the FCFA and the RCFA indicate the presence of quartz (SiO_2), mullite ($3Al_2O_3 \cdot 2SiO_2$), and an amorphous phase which is expressed as an elevated background peak of the difractogram. Traces of anhydrite ($CaSO_4$) were also identified within the FCFA. No clear difference was found in the XRD spectrum between the FCFA and RCFA.

SEM observations reveal that large fractions of the FCFA (5−100 μm particle size) consists of either empty (hollow) spheres, known as cenospheres, or hollow spheres packed with large numbers of smaller spheres, known as plerospheres (*17*). The particle shape deviates from an ideal sphere as the size increases (*18*). At the higher size range (63 to 100 μm), irregular porous "sponge-like" particles were detected. Microcrystals were also observed on the surface of the large cenospheres as well as on the smaller entrapped spheres. RCFA showed similar morphologies but in addition, a new spotty coating was observed. EDS analysis confirmed the XRD results, indicating the presence of mulite, quartz, and the typical plerospheres containing Si, Al, Ca, S, K, and small amounts of Fe. The microcrystals within the FCFA consist of anhydrite ($CaSO_4$), gypsum ($CaSO_4 \cdot 2H_2O$), and carbonate ($CaCO_3$). In general, the mineralogical, chemical, and morphological characteristics of the FCFA particles are similar to those previously described (*3, 5, 18, 21, 22*).

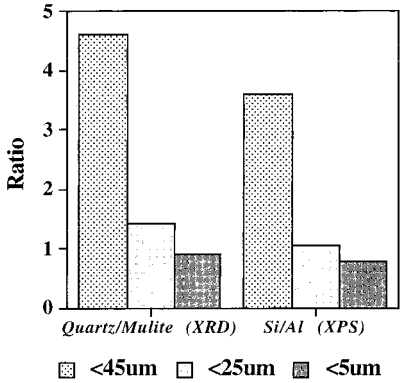

FIGURE 1. Mineralogical and surface chemical composition of different size fractions of FCFA. The ratio between quartz and mulite (measured by XRD) decreased with decreasing particle size. The same trend was detected by the particle surface Si/Al ratios measured by XPS.

XPS results of the surface chemical composition of FCFA and RCFA particles are listed in Tables 1 and 2. We used five samples of 6-month representative ash collected in 1989 and 1991 to characterize the composition of FCFA as the source material dumped to the deep sea. Twenty-one samples from the outer parts of RCFA grains and aggregates were used to study surface chemical changes that occurred after interaction with seawater at ambient conditions. The major components detected in the surfaces of the particles were Al, Si, Ca, Mg, and C. Minor amounts (about 1%) of Fe, Ti, S, K, and P were also identified. Trace element concentrations are detected at the noise levels (*19*) and are not discussed in this paper. In this study, we have normalized the surface element concentrations to Al as a conservative element to minimize the effect of variability in sea salt and carbon contents of the samples and to detect differential dissolution of the major components. Thus, constant element/Al ratios indicate either congruent dissolution/dilution or an inactive chemical system. On the other hand, changes from the original element/Al ratio would be indicative to dissolution or precipitation of phases that do not have the same composition as the bulk.

Mineralogical assembles of FCFA were found to be dependent on particle size distribution (*23*). Our RCFA XRD results revealed that the ratio between quartz and mullite decreased as particle size decreased, in agreement with ref *23*. The same pattern is confirmed by XPS measurements: a decrease in Si/Al ratio with decreasing particle size, reflecting a change in the quartz/mulite ratio (Figure 1).

Comparison between bulk analyses and surface composition of FCFA (Figure 2) indicate surface enrichment of Ca, S, Mg, and P, whereas Ti, Fe, and Si are evenly distributed in CFA (*8*, *10*).

Table 3 presents the average normalized concentrations of surface analyses of FCFA and RCFA, using samples of similar grain size (<45 μm). Significantly lower levels of normalized Ca, S, and Si and higher Mg and Cl were found in the RCFA (Figure 3). Similar changes were observed in the surface of cemented blocks that were exposed to seawater for about 10 years (*9*). No significant differences were observed between RCFA and FCFA for Ti, P, and K. Thus, it appears that Mg, Ca, and S are involved in the main chemical processes that took place on the sea floor.

The 6−8-fold enrichment in Na and Cl in the RCFA is attributed to the presence of sea salt in the samples. The ratio between the two (0.81) is similar to seawater ratio (0.86) and supports this conclusion. Assuming that most of the Cl detected in RCFA (~90%) is of marine origin, we used Cl concentrations to remove the ionic contribution of adsorbed

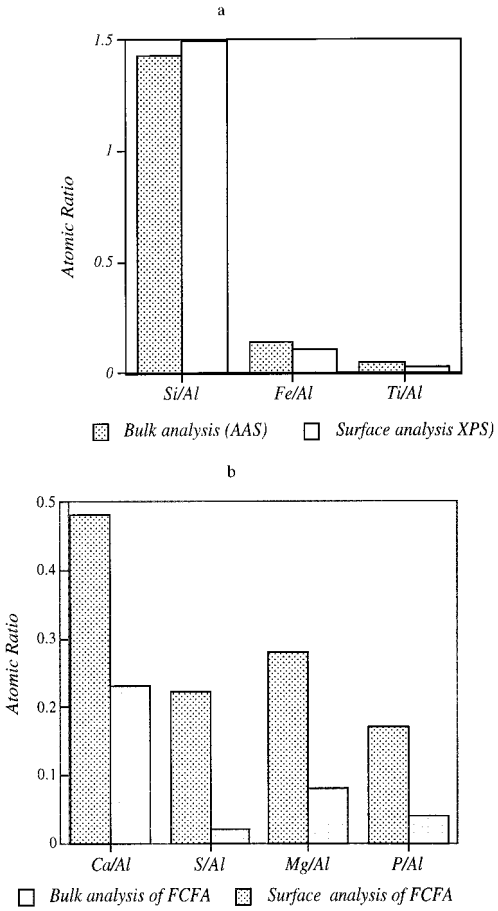

FIGURE 2. Surface and bulk analysis of FCFA, measured by XPS and flame atomic absorption spectroscopy, respectively. The surface was found to be enriched by Ca, S, Mg, and P.

seawater. Thus, the contribution of entrapped or adsorbed seawater to the Mg, Ca and S content in the RCFA were calculated to be negligible.

The decrease in the calcium concentration is accompanied by a decrease in the sulfur concentration. Dissolution of $CaSO_4$ from the FCRA was expected as calcium sulfate phases in seawater are known to be undersaturated (*25*, *26*). While this may account for all sulfur depletion, it cannot explain the Ca depletion, since the ratio of the depleted Ca to S is 4:1 and not 1:1 as expected from the dissolution of calcium sulfate phases. The remaining Ca removal is suggested to be the result of dissolution of other Ca phases such as lime [CaO], portlandite [$Ca(OH)_2$], or amorphous glassy phase (*27*) which can also account for the decrease in Si/Al ratios (Table 3).

The main change in the surface composition is exhibited by more than 1 order of magnitude decrease in the Ca/Mg ratios and an increase of approximately a factor of 5 in the Mg/Al ratios (Table 3). This enrichment can be explained by in situ (authigenic) precipitation of a Mg-phase on the surface of the RCFA particles. We observed the disappearance of the XPS Mg peaks (BDL) in acid-treated RCFA particles.

To examine the properties of this Mg phase, two additional independent analyses were carried out on RCFA samples. The concentration depth profile of Mg in the RCFA particles was studied by using Ar^+ sputtering with the XPS (*10*, *12*, *15*, *29*). A clear reduction in the relative Mg concentration was observed within the first 1−3 min, equivalent to removing 40−120 Å of material. Additional sputtering did not result in a change in the relative Mg concentrations (Figure 4). The Si/Al ratio remained unchanged during the entire depth

TABLE 3. XPS Surface Concentration Ratios (Atomic %) of FCFA and RCFA

sample no.	month	year	Si/Al	Ca/Al	Fe/Al	Ti/Al	S/Al	Mg/Al	P/Al	K/Al	Na/Al	Cl/Al	C/Al	Ca/Mg
1	7−12	1989	1.45	0.49	0.11	0.05	0.20	0.20	0.19	0.05	0.03	nd[a]	2.18	2.48
2	7−12	1989	1.39	0.48	0.10	0.04	0.24	0.36	0.14	0.05	0.03	nd	1.78	1.33
3	7−12	1991	1.31	0.49	0.07	0.03	0.11	0.28	0.13	0.03	0.01	0.03	2.98	1.77
4	7−12	1991	1.23	0.85	0.10	0.05	0.14	0.44	0.07	0.02	0.02	0.05	5.27	1.94
5	1−6	1991	1.61	0.98	0.11	0.07	0.15	0.28	0.15	0.03	0.01	0.06	3.45	3.51
average			**1.40**	**0.66**	**0.10**	**0.05**	**0.17**	**0.31**	**0.14**	**0.04**	**0.02**	**0.04**	**3.14**	**2.21**
SD			0.14	0.24	0.02	0.01	0.05	0.09	0.04	0.01	0.01	0.02	1.36	0.84

sample no.	station	agregate size	Si/Al	Ca/Al	Fe/Al	Ti/Al	S/Al	Mg/Al	P/Al	K/Al	Na/Al	Cl/Al	C/Al	Ca/Mg
12	station P9	<2 cm	1.03	0.27	0.22	0.05	0.10	1.67	0.14	0.08	0.19	0.67	2.34	0.16
13	station P9	<2 cm	0.77	0.26	0.07	0.03	0.09	1.25	0.14	0.03	0.11	0.23	1.39	0.21
14	station P9	<2 cm	1.18	0.38	0.13	0.04	0.10	1.72	0.10	0.06	0.19	0.58	2.57	0.22
15	station P9	<2 cm	1.12	0.29	0.13	0.05	0.09	1.56	0.12	0.04	0.10	0.29	2.35	0.18
25	station P9	2 × 3 mm	1.46	0.11	0.19	0.07	nd	1.19	0.09	0.06	0.17	0.47	2.24	0.09
26	station P9	4 × 5 mm	0.99	0.38	0.14	0.03	0.06	0.83	0.20	0.06	0.14	0.21	1.37	0.46
27	station P9	<2 cm	1.02	0.13	0.12	0.04	0.10	1.66	0.06	0.03	0.07	0.18	2.72	0.08
19	station A	<2 cm	0.84	0.29	0.13	0.05	0.13	1.37	0.10	0.02	0.16	0.39	2.34	0.21
20	station A	<2 cm	0.94	0.31	0.29	0.05	0.08	1.31	0.13	0.03	0.19	0.44	1.93	0.24
21	station A	<2 cm	0.94	0.35	0.11	0.06	0.07	1.49	0.11	0.03	0.13	0.26	2.19	0.23
31	station A	1 cm	0.76	0.60	0.18	0.03	0.17	1.58	0.18	0.04	0.18	0.47	nd	0.38
33	station A	3 cm	1.21	0.13	0.09	0.04	0.12	1.99	0.08	0.02	0.11	0.26	2.28	0.07
34	station A	3 cm	1.13	0.12	0.12	0.06	0.11	1.92	0.07	0.02	0.08	0.21	0.27	0.06
37	trawl	25 × 17 × 13 cm	1.25	0.09	0.17	0.04	0.06	1.82	0.07	0.02	0.08	0.10	1.91	0.05
38	trawl	25 × 17 × 13 cm	1.07	0.09	0.16	0.03	0.10	1.68	0.06	0.03	0.02	0.09	1.53	0.05
average			**1.05**	**0.25**	**0.15**	**0.04**	**0.10**	**1.53**	**0.11**	**0.04**	**0.13**	**0.32**	**2.10**	**0.18**
SD			0.19	0.14	0.06	0.01	0.03	0.31	0.04	0.02	0.05	0.17	0.42	0.12
16	station P9	<2 cm	0.92	0.17	0.10	0.04	0.08	1.18	0.11	bdl[b]	0.06	0.05	1.78	0.14
22	station A	<2 cm	0.92	0.20	0.12	0.04	0.05	1.36	0.10	0.01	0.03	0.02	1.69	0.15
average			**0.92**	**0.18**	**0.11**	**0.04**	**0.07**	**1.27**	**0.11**	**0.01**	**0.04**	**0.04**	**1.74**	**0.14**
SD			0.01	0.02	0.02	0.00	0.03	0.13	0.01		0.02	0.02	0.06	0.00
17	station P9	<2 cm	0.78	0.42	0.04	bdl	0.11	0.77	0.26	bdl	0.04	0.06	21.21	0.54
18	station P9	<2 cm	0.84	nd	nd	nd	0.04	1.22	0.27	nd	nd	0.16	23.24	nd
23	station A	<2 cm	0.71	nd	0.14	0.05	0.02	1.02	0.16	0.006	0.01	bdl	1.10	nd
24	station A	<2 cm	0.67	0.17	0.11	0.05	0.03	0.98	0.14	0.001	0.02	bdl	0.98	0.17
average			**0.75**	**0.29**	**0.09**	**0.05**	**0.05**	**1.00**	**0.21**	**0.004**	**0.02**	**0.11**	**11.63**	**0.36**
SD			0.07	0.18	0.05	0.00	0.04	0.18	0.06	0.004	0.02	0.07	12.26	0.26

[a] nd = not determined. [b] bdl = below detection limit (were not included in the average calculations).

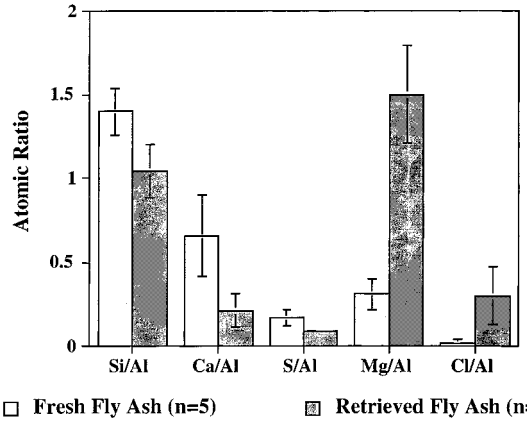

FIGURE 3. Comparison between surface composition of FCFA and retrieved CFA (RCFA). Higher values of Mg and Cl and lower values of Si, Ca, and S were found in the RCFA as compared to the FCFA.

profile (Figure 4). Parallel to the sputtering procedure, relative intensities of two Mg lines, 1s and 2s, were compared. Since a dependence of the attenuation length (λ) on the kinetic energy of the emitted electrons is known (*31*), our goal was to determine the origin of the Mg signal (*30*). A ratio remarkably smaller than one ($R = 0.36$) is found in RCFA indicating that the Mg is buried under a layer devoid of Mg. As a first approximation, a steplike function for the Mg profile was assumed, where beneath a segregation layer the Mg concentration is constant (Figure 5).

With this assumption in mind, the expected intensity ratio will be

$$R_{\text{measured}} \equiv \frac{I_{(\text{Mg}_{1s})}}{I_{(\text{Mg}_{2s})}} = \exp -\left(\frac{d}{\lambda_1} - \frac{d}{\lambda_2}\right) \quad (1)$$

yielding:

$$d = \frac{-\ln(\text{R})}{(1 - \lambda_1/\lambda_2)}\lambda_1 \quad (2)$$

where I is the measured relative concentrations of the different Mg lines, λ is the attenuation length of Mg 1s and 2s which is known to be approximately 13 and 36 Å, respectively (*31*), and d is the thickness of this overlayer. These values correspond to a thickness of approximately 21 Å (Table 4). While the carbon contamination layer is animated to be ~5 Å only, assuming that most of the carbon signal originates from surface contamination (*30*). We also found that applying an exponential model for the Mg distribution (Figure 5) dose not improve the steplike function. Therefore, our results show that the maximum concentration of Mg is found to be at a depth of 21 Å beneath the segregation layer. After sputtering, the Mg concentration is reduced slowly in

TABLE 4. Mg Lines Intensities (1s/2s) and Si/Al and Mg/Al Ratios in a Depth Profile of RCFA Particle in XPS Sputtering Experiment

sputtering time	Mg (1s/2s)	C (1s)	d_0 (Å)	Mg $(1\ s/2s)_{corrected}$	d (Å)	Si/Al	Mg/Al
before sputtering	0.36	11.02	2.5	0.365	21	0.78	1.68
after 1 min of sputtering	0.78	5.00	1.18	0.783	5	0.86	1.55
after 3 min of sputtering	0.79	4.15	0.97	0.801	4.5	0.83	1.26
after 11 min of sputtering	0.75	5.48				0.85	1.01

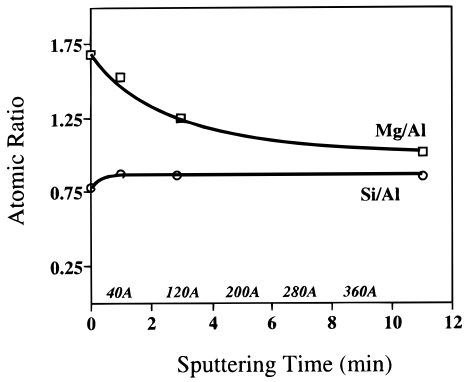

FIGURE 4. XPS sputtering depth profile of Mg/Al and Si/Al ratios in RCFA particles. Mg levels decrease with depth (sputtering time), while Si remains constant. Such behavior indicates the Mg enrichment on the particle surfaces.

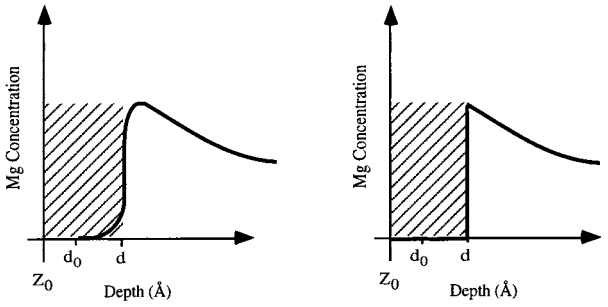

(a) Exponential distribution *(b) Step Function distribution*

FIGURE 5. Schematic presentation of a steplike function and an exponential distribution assumptions for the Mg profile in RCFA particles. These models were used to estimate the depth of the coating Mg layer (see text).

a range of 130 Å to its asymptotic bulk concentration. Furthermore, since the Ar^+ ion beam is not normal to the surface and the material is porous, parts of it was not exposed to the incoming ions. The XPS, on the other hand, impinges at 90° and therefore it samples the entire surface. We estimated that only ~62% of the surface was sputtered.

The second indication for surface formation of a Mg phase on the RCFA is given by the XPS analysis of O (1s) line width. It has been previously suggested that the shape and width of the O (1s) line, derived from the XPS spectra, may be important in monitoring atomic level structural changes that may occur on silicate mineral and glass surfaces during reaction with aqueous solutions (*6, 30*). It was shown that the O (1s) peak depends on the neighboring oxygen atoms; therefore, glass has a significantly wider O (1s) peak than a crystal containing oxygen. Our XPS results indicate that upon seawater interactions, the full width at half-maximum (fwhm) of O (1s) decreases from 2.50 ± 0.07 for FCFA to 2.26 ± 0.06 in RCFA. Precipitation of a Mg crystallized phase is expected to support this trend since the oxygen environment would change from an amorphous to a crystalline one.

It is suggested that precipitation of a new Mg phase has occurred on the surfaces. This phase is believed to be Mg-$(OH)_2$—brucite. A similar explanation was suggested for the Mg enrichment in coal combustion waste with scrubber sludge − SSFA by Seligman and Duedall (*26*) or in cement stabilized CFA as described by Hockley and van Der Sloot (*9*). The same morphology, as identified in this work, was also observed on quartz particles, within an alkaline solution containing 10^{-3} M $MgCl_2$ (*28*). We suggest the following mechanism to explain the observed results. In the case of CFA class C (alkaline CFA), it is expected that as a result of rapid hydrolysis interactions with seawater, the pH at the boundary layer solution will be very high (>11) (*27*). Dissolution of the silicate phase will be enhanced by the high pH (*33*), resulting in a decrease in Si concentrations. An alkaline boundary layer around the CFA particles and the Mg concentration in seawater (~53 mM) creates a saturated solution with respect to brucite—$Mg(OH)_2$ (s) (*33*), leading to precipitation of this phase on the particle surfaces.

The XPS comparison between FCFA and RCFA were performed on particles in the size fraction of <45 μm. Two additional fractions of the retrieved material, 20 and 5 μm, were analyzed. In general, the results follow the basic chemical trends comparing FCFA and RCFA and suggest that all the above processes are applicable for all size fractions. However, some differences occur among the RCFA fractions. The decrease of normalized Ca, Si, S, Mg, Na, and Cl with decreasing particle size indicate enhanced dissolution of the small particles. We suspect that this dissolution might have occurred during laboratory processing of the samples as the Na and Cl exhibit values of the FCFA (complete wash of seasalts) and the other phases dissolved in the freshwater. We cannot exclude the possibility that part of this dissolution (except for the Mg phase) took place under deep-sea conditions due to the high specific surface area of the particles.

The interaction between CFA and seawater that leads to precipitation of the Mg phase on the surfaces and the dissolution of Ca and amorphous Si phases may have some implication to the leaching of toxic heavy metals in deep sea disposal sites. In general, dissolution of CFA is expected to release heavy metals due to their high concentration in CFA. However, the formation of Mg layers under elevated pH conditions may inhibit heavy metals release from these surfaces. Further work is required in the future to establish XPS methodology for trace element measurements and to quantify the importance of such a process.

Acknowledgments

The authors express their gratitude to the crew of the R/V *Shikmona*. This study was partly supported by the Israel Ministry of National Infrastructures and the Israel Ministry of the Environment.

Literature Cited

(1) Bamber, R. M. *Mar. Pollut. Bull.* **1980**, *11*, 323−326.
(2) Crecelius, E. A. Fly ash disposal in the ocean: an alternative worth considering. In *Waste in the ocean*; 1985, John Wiley & Sons: New York, 1985; pp 379−388.

(3) Theis, T. L.; Gardner, K. H. *Crit. Rev. Environ. Control* **1990**, *20*, 21−42.
(4) Carlson, C. L.; Adriano, D. C. *Environ. Qual.* **1993**, *22*, 227−247.
(5) Grisafe, D. A.; Angino, E. E.; Smith, S. M. *Appl. Geochem.* **1988**, *3*, 601−608.
(6) Sloot, H. A. v. d.; Hoek, E. E. v. d.; Groot, G. J. D.; Comans, R. N. J. *Classification Of Pulverized Coal Ash Part 1. Leaching behaviour of coal fly ash*; Netherland Energy Research Foundation (ECN) Report (R92004); ECN: Amsterdam, The Netherlands, 1992; 23 pp.
(7) Kress, N.; Golik, A.; Galil, B.; Krom, M. D. *Mar. Poll. Bull.* **1993**, *26*, 447−456.
(8) Harvey, E. S. *Oceanic Processes Mar. Poll.* **1991**, *3*, 85−98.
(9) Hockley, D. E.; Van Der Sloot, H. *Environ. Sci. Technol.* **1991**, *27*, 1408−1414.
(10) Hochella, M. F.; Lindsay, J. R.; Mossotti, V. G.; Eggleston, C. M. *Am. Mineral.* **1988**, *73*, 1449−1456.
(11) Hochella, M. F. Auger electron and X-ray photoelectron Spectroscopies. *Rev. mineral.* **1988**, 573−673.
(12) Campbell, J. A.; Smith, R. D.; Davis, L. E. *Appl. Spectrosc.* **1978**, *32*, 316- 319.
(13) Kawai-J.; Hayakawa-S.; Zheng-SY, E.-F.; Kitajima-Y.; Maeda-K.; Adachi-H.; Gohshi-Y.; Furuya-K *Anal. Chem.* **1995**, *67*, 1526−1529.
(14) Hirokawa, K.; Danzaki, Y. *Surf. Interface Anal.* **1984**, *6*, 193−195.
(15) Ersez, T.; Liesegang, J. *Appl. Surf. Sci.* **1991**, *51*, 35−46.
(16) Bogdanovic, I.; Fazinic, S.; Itskos, S. *Nucl. Instrum. Methods Phys. Res.* **1995**, *99*, 402−405.
(17) Fisher, G. L.; Chang, D. P. Y. *Science* **1976,** *192*, 553−555.
(18) Schure, M. R.; Solty, P. A.; Natusch, D. F. S.; Mauney, T. *Environ. Sci. Technol.* **1984**, *19*, 82−86.
(19) Hoek, E. E. v. d.; Bonouvrie, P. A.; Comans, R. N. J. *Appl. Geochem.* **1994**, *9*, 403−412.
(20) Sherwood, P. M. A. *Data Analysis in XPS and AES*. In *Practical Surface Analysis*; Briggs, D., Seah, M. P. John Wiely & Sons Ltd: New York, 1990.
(21) Grossman, S.; Natan, Y.; A, M. *J. Coal Quality* **1988**, *7*, 22−26.
(22) Fisher, G. L.; Pentice, B. A.; Silberman, D. *Environ. Sci. Technol.* **1978**, *12*, 447- 451.
(23) Hulett, L. D.; Weinberger, A. J. *Environ. Sci. Technol.* **1980**, *14*, 965−970.
(24) Windom, H. L. *Environ. Sci. Technol.* **1989**, 23, 314−320.
(25) Roethel, F. J. Effects of seawater on the mineralogical and chemical composition of coal-waste Blocks. In *Waste in the ocean*; John Wiley & Sons: New York, 1985; pp 692−715.
(26) Seligman, J. D.; Duedall, L. W. *Environ. Sci. Technol.* **1979**, *13*, 1082−1086.
(27) Schramke, J. A. *Appl. Geochem.* **1992**, *7*, 481−492.
(28) Krishnan, S. V.; Iwasaki, I. *Environ. Sci. Technol.* **1986**, *20*, 1224−1229.
(29) Faure, G., *Principles and Applications of Inorganic Geochemistry*; Macmillan Publishing Company: New York, 1991.
(30) Hofmann, S. Depth Profiling in AES and XPS. In *Practical Surface Analysis*; Briggs, D., Seah, M. P., Eds.; John Wiley & Sons Ltd.: New York, 1990; pp 143−199.
(31) Seah, M. P. *Quantification of AES and XPS*. In *Practical Surface Analysis*; Briggs, D., Seah, M. P., Eds.; John Wiley & Sons Ltd.: New York, 1990; pp 201−255.
(32) Hochella, M. F.; Brown, G. E. *Geochim. Cosmochim. Acta*. **1974**, *52*, 1641−1648.
(33) Stumm, W.; Morgan, J. J. *Aquatic Chemistry*; John Wiley & Sons: New York, 1981; pp 540−542.

Received for review June 2, 1998. Revised manuscript received October 12, 1998. Accepted October 19, 1998.

ES9805573